Chapter 5

Nonclassicalities in $\mathcal{PT}$ −Symmetric coupled micro-cavities

5.1 Introduction

The idea of parity-time-symmetry ($\mathcal{PT}$ −symmetry) is very interesting as well as important to discuss different optical and optomechanical quantum phenomena. In last few decades, the attentiveness of the researcher has been taken by it. Bender and Boettcher [167] first gave the concept about it in 1998. They have shown that a non-Hermitian Hamiltonian possesses real eigenvalues if the Hamiltonian obeys $\mathcal{PT}$ −symmetry. Generally, Hermitian Hamiltonian has real eigenvalues and wave-functions are orthogonal. On the other hand, non-Hermitian Hamiltonian possesses complex eigenvalues and wave-functions are biorthogonal. For a wave-function, the quantitative measure of biorthogonality with respect to orthogonality is called as phase rigidity. The $\mathcal{PT}$ −symmetry of a Hamiltonian indicates $[H, \mathcal{PT}] = 0$ i.e. the Hamiltonian commutes with joint combination of unitary parity ($\mathcal{P}$) operator and anti-unitary time reversal ($\mathcal{T}$) operator.

The idea of $\mathcal{PT}$ −symmetry begins with a mathematical ground but it has been experimentally demonstrated and also theoretically analyzed in different optical systems with potential applications and it also opens a new platform to study different quantum mechanical aspects. The different optomechanical or optical effects are studied via $\mathcal{PT}$ −symmetry such as non-reciprocal propagation of light [168], lasing action based on polarisation [169], OMIT in micro-resonators [170], topological energy transfer [171], sensitivity enhancement [172], slow light [173] etc. It is also explored via different advanced topics in physics such as electronic LCR circuit [174], metamaterials [175], acoustics [176], quantum electrodynamics [177] etc.

The $\mathcal{PT}$ −symmetric system is analyzed in this chapter is an OQS. The OQSs have connection with environment and are associated with loss and gain. This type of system experiences a phase transition – unbroken $\mathcal{PT}$ −symmetry phase with real eigenvalues to broken $\mathcal{PT}$ −symmetry phase with complex eigenvalues. The non-analytical transition point is known as EP. At this point $\mathcal{PT}$ −symmetry is spontaneously broken. Different optical phenomenons are changed significantly during the transition.

The affect of $\mathcal{PT}$ −symmetry theory on different nonclassicalities has not been extensively studied till now. Enhancement photon blockade effect was theoretically studied by Li et al [178] in recent past, via $\mathcal{PT}$ −symmetry theory. Here we have explored different nonclassical features such as single and compound mode squeezing, intermodal entanglement and EPR steering, in the context of $\mathcal{PT}$ −symmetry theory. We have also discussed how the degree of nonclassicalities is influenced by $\mathcal{PT}$ −symmetry phase transition.

5.2 Model Hamiltonian

The model system has two micro-cavities [178] as depicted in figure 5.1. One micro-cavity is passive, with total loss rate k_1 . The total loss rate is based on two losses – external coupling loss and intrinsic loss. This cavity contains optical Kerr medium (3^{rd} order nonlinear susceptibility). Other micro-cavity is active, with actual loss rate k_2 . The actual loss rate is sum of round-trip energy gain rate and intrinsic rate. The value of the loss rate k_2 may be negative (gain) positive (loss), depending on the rate of round-trip energy gain. Depending upon gain-to-loss ratio, the present system shows two possible arrangements (i) passive-passive cavity system (PPCS) - k_1 and k_2 both are positive (ii) passive-active cavity system (PACS) - k_1 is positive and k_2 is negative.

The PACS is known as $\mathcal{PT}$ −symmetric system. The two micro-cavities are coupled through photon tunnelling strength J . The tunnelling rate depends on the separation between the two micro-cavities. The Hamiltonian of the system is

$$H = H_s + H_{int} + H_{nl} + H_d \tag{5.1}$$

The total Hamiltonian contains four parts. First part present Hamiltonian of both passive and active cavity with resonance frequencies ω_{a_1} and ω_{a_2}, respectively. $a_1\ (a_1^\dagger)$ and $a_2\ (a_2^\dagger)$ are the destruction (creation) operators for passive and active field modes, respectively. Second part represents interaction via photon tunnelling between the cavities. Third one is due to passive nonlinear Kerr medium (strength U) placed inside the cavity. Last part indicates driving term with strength Ω and driving frequency ω_d . The details of all the parts are as follows:

$$H_s = \begin{pmatrix} a_1^\dagger & a_2^\dagger \end{pmatrix} \begin{pmatrix} \omega_{a_1} - \frac{ik_1}{2} & 0 \\ 0 & \omega_{a_2} - \frac{ik_2}{2} \end{pmatrix} \begin{pmatrix} a_1 \\ a_2 \end{pmatrix}$$

$$H_{int} = \begin{pmatrix} a_1^\dagger & a_2^\dagger \end{pmatrix} \begin{pmatrix} 0 & J \\ J & 0 \end{pmatrix} \begin{pmatrix} a_1 \\ a_2 \end{pmatrix}$$

$$H_{nl} = U{a_1}^{\dagger 2}{a_1}^2 \text{ and } H_d = \Omega {a_1}^\dagger e^{-i\omega_d t} + h.c.$$

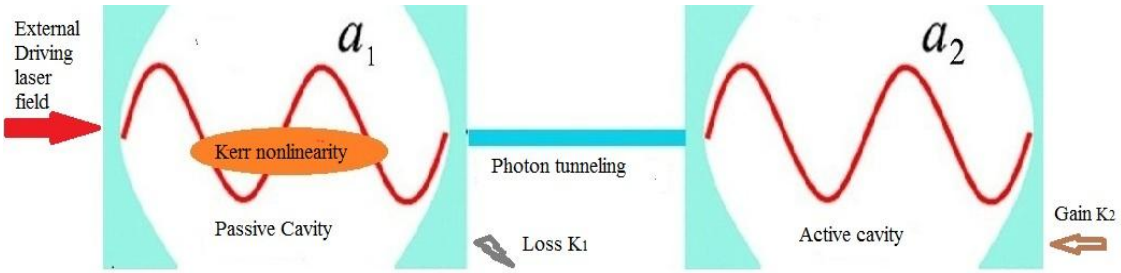

Figure 5.1: Schematic diagram of the model system

For a coupled WGM micro-toroidal resonator set up, one is designed from silica material without gain-medium and dopants i.e. passive loss where the electric field contain third-order nonlinear interaction term. Another micro-toroid is fabricated from silica doped with Er^{3+} ions, used as active resonator. One can achieve 1550 nm band in active micro-toroidal system via optical gain by using pump laser of 1460 nm wavelength (for optical pumping of Er^{3+} ions). The evanescent coupling in between two micro-toroid systems is at 1550 nm band but no coupling is possible for 1460 nm band. There is no similar resonance line of 1460 nm. So, pump laser input is incorporated with the active micro-toroid only [179].

The different system parameters are as follows: In a passive microtoroid system loss rate is $\sim 2\pi \times 10.7$ MHz and coupling quality factor is $\sim 4.5 \times 10^7$. The loss rate can also be tuned by changing taper-resonator gap. In active microtoroid system the gain rate is $\sim -2\pi \times 10.7$ MHz. The photon tunnelling strength between two microtoroids is $\sim 2\pi \times 5.35$ MHz. For silica glass material the Kerr nonlinear strength is $\sim 2\pi \times 1.07$ MHz. The gain-to-loss ratio varies from -3 to $+3$ [180 -185] and also references there in.

5.3 Details of parity-time-symmetry theory

The detail of $\mathcal{PT}$ −symmetry mechanism [178] of the present system is illustrated as follows: In absence of driving and weak Kerr nonlinear strength. The Hamiltonian becomes

$$\mathcal{H} = \begin{pmatrix} a_1^\dagger & a_2^\dagger \end{pmatrix} \begin{pmatrix} \omega_{a_1} - \frac{ik_1}{2} & J \\ J & \omega_{a_2} - \frac{ik_2}{2} \end{pmatrix} \begin{pmatrix} a_1 \\ a_2 \end{pmatrix}$$

After diagonalization the above Hamiltonian and some tedious calculations the eigenvalues are obtained as

$$\omega_{\pm} = \frac{1}{2}\left(\omega_{a_1} + \omega_{a_2} - i\frac{k_1 + k_2}{2}\right) \pm \frac{1}{2}\sqrt{4J^2 - \left[i\left(\omega_{a_1} - \omega_{a_2}\right) + \frac{k_1 - k_2}{2}\right]^2}$$

From the above expressions of $\omega_{\pm}$, it is clear that eigenfrequencies are determined by cavity resonance frequencies, cavity loss and gain rates and photon tunnelling rate. The eigenvalues are real if the imaginary part of $\omega_{\pm}$ vanishes. The values of $\omega_{\pm}$ are real when $\omega_{a_1} = \omega_{a_2}$, $k_2 = -k_1$ and $J \geq \frac{k_1}{2}$. The relation $k_2 = -k_1$ indicates the balanced loss and gain, $\omega_{a_1} = \omega_{a_2} = \omega_0$ specify the same resonance frequencies. In this case the eigenvalues become $\omega_{\pm} = \omega_0 \pm \frac{1}{2}\sqrt{4J^2 - {k_1}^2}$. So, $\mathcal{PT}$ −symmetry super-modes are spatially separated by $\frac{1}{2}\sqrt{4J^2 - {k_1}^2}$, from both sides of the ω_0 . When $J = \frac{k_1}{2}$, the two super-modes merge into the frequency ω_0 . For the case of $J < \frac{k_1}{2}$, the values $\omega_{\pm}$ are complex and the system is in $\mathcal{PT}$ −symmetry broken phase. At this phase, one of two super-modes successively disappears due to absorption and at the same time other undergoes amplification. When $J > \frac{k_1}{2}$, the system is in unbroken phase. So, $J = \frac{k_1}{2}$ is known as exceptional point (EP) or transition point.

5.4 Analytical Solutions

For simplicity, we consider the Hamiltonian in absence of driving term. So, system Hamiltonian takes the form

$$H' = \left(\omega_{a_1} - \frac{ik_1}{2}\right)a_1^{\dagger}a_1 + \left(\omega_{a_2} - \frac{ik_2}{2}\right)a_2^{\dagger}a_2 + J\left(a_1^{\dagger}a_2 + h.c.\right) + U{a_1}^{\dagger 2}{a_1}^2 \qquad (5.2)$$

The Heisenberg EOM corresponds to passive and active cavity field modes are given by

$$\dot{a_1}(t) = -i\left[\left(\omega_{a_1} - \frac{ik_1}{2}\right)a_1(t) + Ja_2(t) + 2Ua_1^{\dagger}(t)a_1^2(t)\right]$$

$$\dot{a_2}(t) = -i\left[\left(\omega_{a_2} - \frac{ik_2}{2}\right)a_2(t) + Ja_1(t)\right] \tag{5.3}$$

We assume the solutions of the above equations (5.3) are

$$a_1(t) = A_1a_1(0) + A_2a_2(0) + A_3a_1^{\dagger}(0)a_1^2(0) + A_4a_1(0) + A_5a_1^2(0)a_2^{\dagger}(0) + A_6a_1^{\dagger}(0)a_1(0)a_2(0) + A_7a_1^{\dagger}(0)a_1^2(0) + A_8a_1^{\dagger 2}(0)a_1^3(0)$$

$$a_2(t) = B_1a_2(0) + B_2a_1(0) + B_3a_2(0) + B_4a_1^{\dagger}(0)a_1^2(0) \tag{5.4}$$

A_i and B_i are the function of time and also depend on loss rate, gain rate, photon tunneling rate, nonlinear strength and frequency. These are found out from boundary condition $A_1(0) = B_1(0) = 1$ and $A_i(0) = 0$ for $i = 2, \dots, 14$ and $B_i(0) = 0$ for $i = 2, \dots, 4$ (corresponding equations are in appendix C). These are as follows:

$$A_1 = e^{-i(\omega_{a_1} - \frac{ik_{a_1}}{2})t}$$

$$A_2 = \frac{J}{\omega'}A_1(1 - e^{i\omega' t})$$

$$A_3 = -2iUtA_1$$

$$A_4 = -\frac{J^2}{(\omega_b - \frac{ik_b}{2})\omega'}A_1\left[e^{-i(\omega_b - \frac{ik_b}{2})t} + i\left(\omega_b - \frac{ik_b}{2}\right) - 1\right]$$

$$A_5 = -\frac{2UJ}{\omega'^2}A_1(e^{-i\omega' t} + i\omega' t)$$

$$A_6 = -\frac{4UJ}{\omega'^2}A_1(e^{i\omega' t} - i\omega' t - 1)$$

$$A_7 = A_8 = -2U^2t^2A_1$$

$$B_1 = e^{-i(\omega_{a_2} - \frac{ik_{a_2}}{2})t}$$

$$B_2 = \frac{J}{\omega'}B_1(e^{-i\omega' t} - 1)$$

$$B_3 = \frac{J^2}{\omega'^2} B_1 (e^{i\omega' t} + i\omega' t - 1)$$

$$B_4 = \frac{2UJ}{\omega'^2} B_1 \{1 - e^{-i\omega' t}(1 + i\omega' t)\} \quad (5.5)$$

Where $\omega' = \left(\omega_{a_1} - \omega_{a_2}\right) - \left(\frac{ik_{a_1}}{2} - \frac{ik_{a_2}}{2}\right)$

To check the sustainability of the solutions we have employed equal time commutation relation $\left[a_i(t), a_j(t)\right] = \delta_{ij}$. To calculate different nonclassical correlation factors, we assume initial state as the product of coherent states. So, initial state $\varphi = |\, \alpha_1\rangle \otimes |\, \alpha_2\rangle$ where $|\, \alpha_1\rangle$ and $|\, \alpha_2\rangle$ are the eigenkets of passive cavity field operator a_1 and active cavity field operator a_2 respectively. The operator $a_1(t)$ operates on the product state, it results complex eigenvalue α_1 .

5.5 Numerical Solutions

To account the presence of driving term we have used Lindblad's master equation. The equation is given by

$$\dot{\rho} = -i[H, \rho] + \mathcal{L}(\rho) \quad (5.6)$$

Where $\mathcal{L}(\rho) = \mathcal{L}_{a_1}(\rho) + \mathcal{L}_{a_2}(\rho)$; $\mathcal{L}_a(\rho)$ is expresses by the following relation $(a \in a_1, a_2)$

$$\mathcal{L}_a(\rho) = \frac{k_i}{2}(n_a^T + 1)(2a\rho\, a^\dagger - a^\dagger a\rho - \rho\, a^\dagger a) + \frac{k_i}{2} n_a^T (2a\rho\, a^\dagger - a^\dagger a\rho - \rho\, a^\dagger a)$$

with k_i is the loss rate or gain rate of the cavity field modes and n_a^T is thermal photon number.

In rotating frame at the driving field frequency ω_d, the Hamiltonian of the system is transformed by $U(t) = \exp\{-i\omega_d(a_1^\dagger a_1 + a_2^\dagger a_2)t\}$ and it takes the following form

$$H_r = \Delta_{a_1} a_1^\dagger a_1 + \Delta_{a_2} a_2^\dagger a_2 + J\left(a_1 a_2^\dagger + a_1^\dagger a_2\right) + U {a_1}^{\dagger 2} {a_1}^2 + \Omega({a_1}^\dagger + a_1) \quad (5.7)$$

Where $\Delta_a = \omega_a - \omega_d$ is frequency detuning between cavity field and driving field. To obtain numerical solution we consider initial state as Fock state basis ($|n_{a_1}\rangle \otimes |n_{a_2}\rangle$) where $n_{a_1}$and n_{a_2} are the cavity photon numbers of the passive and active field mode, respectively. For generality, we assume both the cavity field mode have same detuning i.e. $\Delta_{a_1} = \Delta_{a_2} = \Delta$ and average thermal photon number is zero i.e. $n_a^T = 0$.

5.6 Quadrature Squeezing

We illustrate the possibilities of different types of squeezing effects by using both analytical and numerical solutions. The dependence of squeezing factors on different system parameters are reported for both single and compound field mode, in detail.

5.6.1 Single mode Squeezing

We examine the possibility of single mode squeezing by using quadrature operators (equation 2.6) and solutions of equation (5.4). The variance of the field quadratures are obtained as follows:

$$\begin{pmatrix}(\Delta X_{a_1})^2\\(\Delta Y_{a_1})^2\end{pmatrix} = \frac{1}{4}[1 + A_2^* A_2 + 2A_3^* A_3|\alpha_1|^2(1 + 2|\alpha_1|^2) + (2A_1^* A_3|\alpha_1|^2 + 2A_1^* A_5\alpha_1\alpha_2{}^* + A_1^* A_6\alpha_1{}^*\alpha_2 + A_1^* A_4 + 2A_1^* A_7|\alpha_1|^2 + 3A_1^* A_8|\alpha_1{}^2|^2 + c.c.) \pm (A_1A_3\alpha_1{}^2 + 2A_3^2\alpha_1{}^*\alpha_1{}^3 + A_1A_6\alpha_1\alpha_2 + A_1A_7\alpha_1{}^2 + 2A_1A_8\alpha_1{}^*\alpha_1{}^3 + c.c.)] \quad (5.8)$$

$$\begin{pmatrix}(\Delta X_{a_2})^2\\(\Delta Y_{a_2})^2\end{pmatrix} = \tfrac{1}{4}\{1 + B_2^* B_2 + (B_3^* B_1 + c.c.)\} \quad (5.9)$$

Equation (5.8) and (5.9) correspond to quadrature variance of passive and active cavity field mode, respectively. From these, it is clear that squeezing is possible for passive cavity field mode. For active cavity field mode there is no signature of squeezing.

Temporal variation of the field quadratures of equation (5.8), is depicted in figure 5.2 (a-c) with different gain-to-loss ratio, photon tunnelling strength.

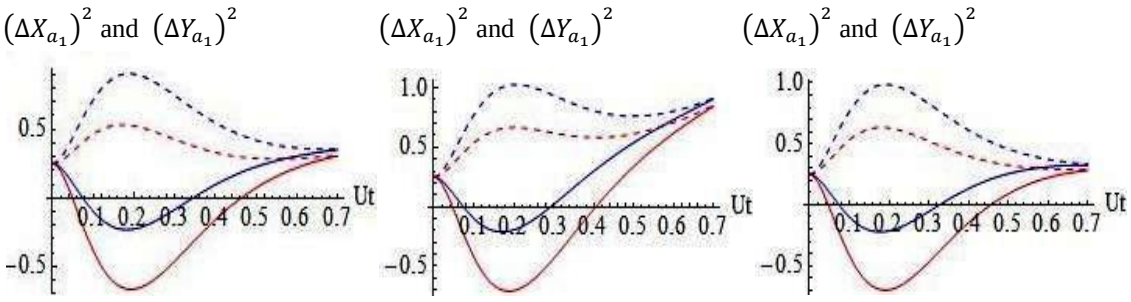

(a) (b) (c)

Figure 5.2: Variation of the variance of the field quadratures $(\Delta X_{a_1})^2$ (solid line) and $(\Delta Y_{a_1})^2$ (dashed line) with normalised time Ut. The parameters are $|\alpha_1| = 2$, $|\alpha_2| = 1$ (blue) ; $|\alpha_1| = 2$, $|\alpha_2| = 2$ (red) (a) $J/k_1 = 0.2$, $k_2/k_1 = -0.2$ (b) $J/k_1 = 0.5$, $k_2/k_1 = 0.2$ (c) $J/k_1 = 0.5$, $k_2/k_1 = -0.2$.

Figure 5.2(a) corresponds to broken $\mathcal{PT}$ −symmetry regime (passive-active system) whereas figure 5.2(b) and (c) represent the variation for PPCS and PACS at unbroken $\mathcal{PT}$ −symmetry regime. The degree of squeezing is pronounced at unbroken phase as compared to broken phase.

To study higher order single mode squeezing effect in present system we use higher order field quadrature operators (equation 2.11) and solutions of the field operators of equation (5.4). For simplicity, here we have studied amplitude squared squeezing and obtained the following analytic expression of the squeezing factors.

$$\begin{aligned}\binom{S_1}{S_2} = \frac{1}{4}[&\{4A_2^*A_2(1+|\alpha_1|^2) + 2A_3^*A_3(17|{\alpha_1}^3|^2 + 44|{\alpha_1}^2|^2 + 20|\alpha_1|^2 + 1)\\ &+ 4A_3^{*2}A_1^2|\alpha_1|^2(2|{\alpha_1}^2|^2 + 6|\alpha_1|^2 + 3) + 4A_2^*A_3\alpha_1{\alpha_2}^*(2|\alpha_1|^2 + 1)\\ &+ 2A_3^*A_1(4|{\alpha_1}^2|^2 + 8|\alpha_1|^2 + 1) + 4A_4^*A_1(|\alpha_1|^2 + 1)\\ &+ 4A_5^*A_1{\alpha_1}^*\alpha_2(2|\alpha_1|^2 + 3) + 4A_6^*A_1\alpha_1{\alpha_2}^*(|\alpha_1|^2 + 4)\\ &+ 2A_7^*A_1(4|{\alpha_1}^2|^2 + 8|\alpha_1|^2 + 1) + 8A_2^{*2}A_1^2|\alpha_1|^2\alpha_1{\alpha_2}^*\\ &+ 4A_2^*A_3^*A_1^2\alpha_1{\alpha_2}^* + 12A_8^*A_1|\alpha_1|^2(|{\alpha_1}^2|^2 + 3|\alpha_1|^2 + 1) + c.c\}\\ &\pm\{4A_3A_1^3{\alpha_1}^4 + 4A_6A_1^3{\alpha_1}^3\alpha_2 + 4A_7A_1^3{\alpha_1}^4 + 8A_8A_1^3{\alpha_1}^4(|\alpha_1|^2 + 1)\\ &+ 2A_3^2A_1^2{\alpha_1}^4(8|\alpha_1|^2 + 5) + 8A_2A_3A_1^2{\alpha_1}^3\alpha_2 + c.c.\}] \qquad (5.10)\end{aligned}$$

Figure 5.2(a-d) displays the time evolution of the amplitude squared squeezing factors for different photon tunnelling strength and gain-to-loss ratio. The variation of squeezing factors of PACS at broken $\mathcal{PT}$ −symmetry regime is shown in figure 5.2(a). The same variation is presented in figure 5.2(b) and (c) correspond to PPCS and PACS at EP, respectively. Figure 5.2(d) depict the same at unbroken $\mathcal{PT}$ −symmetry regime for PACS. Here one field quadrature is always squeezed due to expense of other quadrature. The negativity of the field quadrature increases with photon tunnelling strength. The degree of amplitude squared squeezing is more pronounced as compared to lower order squeezing.

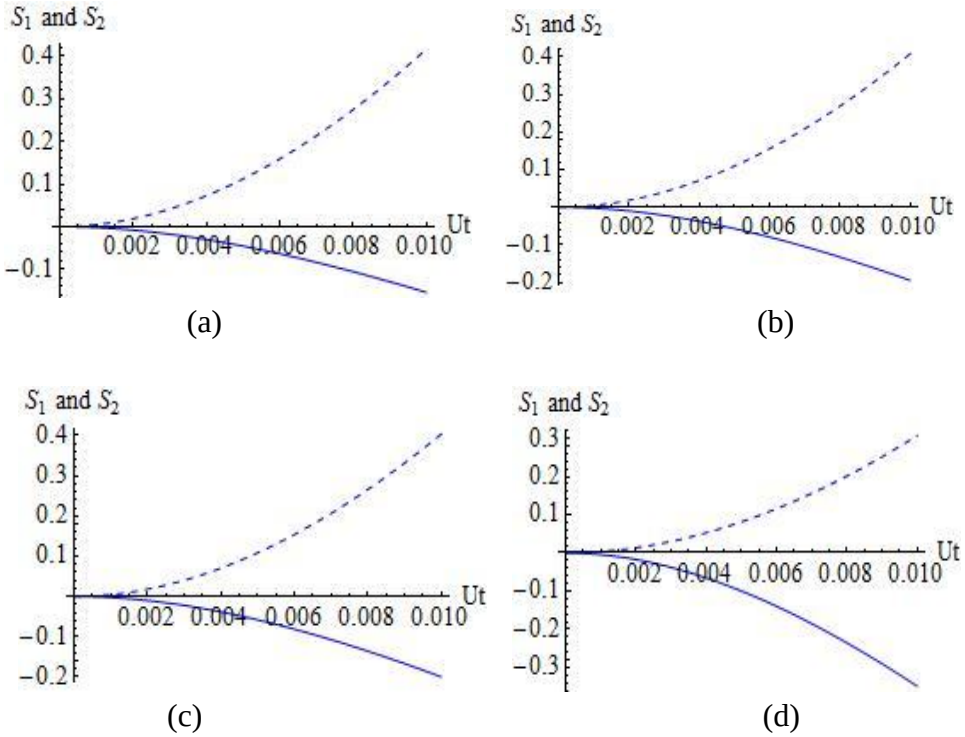

Figure 5.3: Variation of amplitude squared squeezing factors S_1 (solid line) and S_2 (dashed line) with Ut. The parameters are $|\alpha_1| = 2,\ |\alpha_2| = 1$ (a) $J/k_1 = 0.2$, $k_2/k_1 = 0.2$ (b) $J/k_1 = 0.5,\ k_2/k_1 = 0.2$ (c) $J/k_1 = 0.5,\ k_2/k_1 = -0.2$ and (d) $J/k_1 = 1.0, k_2/k_1 = -0.2$.

5.6.2 Compound mode squeezing

Using solutions of equation (5.4) and compound mode quadrature (equation 2.7 and 2.8), we obtain the expression of the variance of the field quadratures as follows:

$$\begin{pmatrix}(\Delta X_{a_1a_2})^2\\(\Delta Y_{a_1a_2})^2\end{pmatrix} = \frac{1}{8}[2 + A_2^*A_2 + 2A_3^*A_3|\alpha_1|^2(1+2|\alpha_1|^2) + B_2^*B_2$$
$$+ (A_1^*A_4 + A_1^*A_3 + A_2^*B_1 + 2A_1^*A_3|\alpha_1|^2 + 2A_1^*A_5\alpha_1\alpha_2{}^* + A_1^*A_6\alpha_1{}^*\alpha_2$$
$$+ 2A_1^*A_7|\alpha_1|^2 + 3A_1^*A_8|\alpha_1{}^2|^2 + 2A_1^*B_4|\alpha_1|^2 + 2A_3^*B_2|\alpha_1|^2$$
$$+ A_6^*B_1|\alpha_1|^2 + c.c.)$$
$$\pm (A_1A_3\alpha_1{}^2 + 2A_3^2\alpha_1{}^*\alpha_1{}^3 + A_1A_6\alpha_1\alpha_2 + A_1A_7\alpha_1{}^2 + 2A_1A_8\alpha_1{}^*\alpha_1{}^3$$
$$+ A_3B_2\alpha_1{}^2 + A_1B_4\alpha_1{}^2 + A_5B_1\alpha_1{}^2 + c.c.)] \qquad (5.11)$$

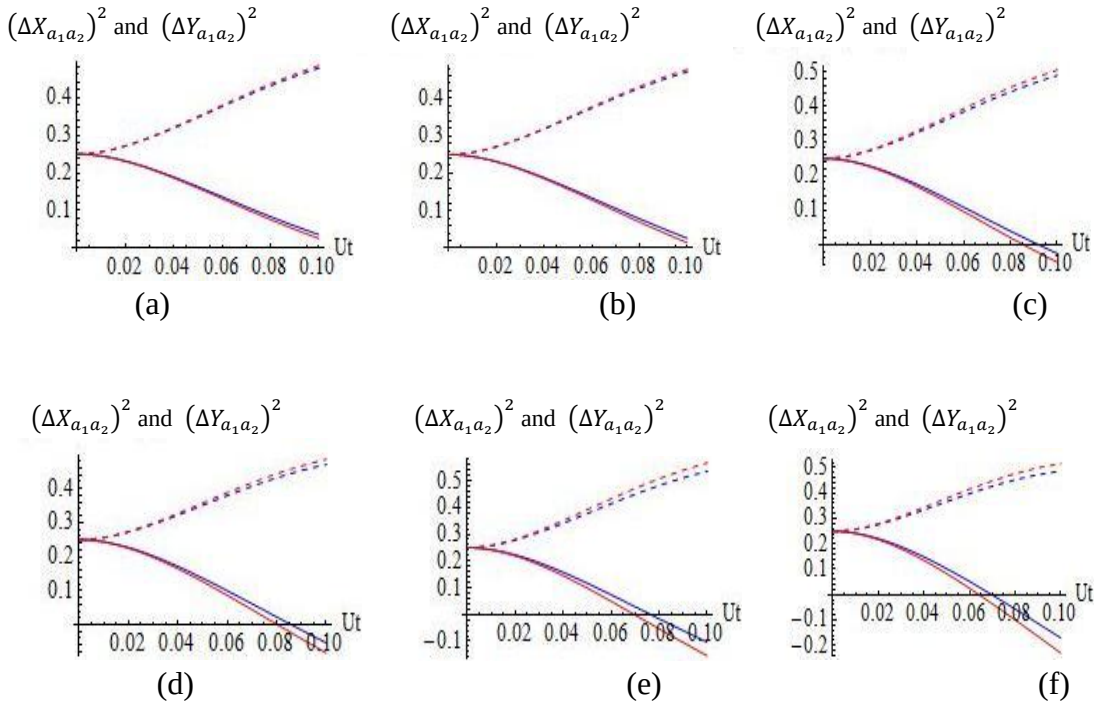

Figure 5.4: Variation of $(\Delta X_{a_1a_2})^2$ (solid line) and $(\Delta Y_{a_1a_2})^2$ (dashed line) with normalised time Ut. The parameters are $|\alpha_1| = 2$, $|\alpha_2| = 1$ (blue) ; $|\alpha_1| = 2$, $|\alpha_2| = 2$ (red) (a) $J/k_1 = 0.2,\ k_2/k_1 = 0.2$ (b) $J/k_1 = 0.2,\ k_2/k_1 = -0.2$ (c) $J/k_1 = 0.5,\ k_2/k_1 = 0.2$ (d) $J/k_1 = 0.5,\ k_2/k_1 = -0.2$ (e) $J/k_1 = 1.0,\ k_2/k_1 = 0.2$ (f) $J/k_1 = 1.0,\ k_2/k_1 = -0.2$.

From inspection of equation (5.11), it is observed that squeezing is possible for passive and active cavity inter field mode. To study the fluctuation of field quadratures, we plot the right side of equation (5.11) as a function of normalised time Ut in figure 5.4 (a-f). Figure 5.4(a) and (b) represent the quadrature variation for PPCS and PACS at broken regime. The same variation is depicted in figure 5.4(c-d) and 5.4(e-f) correspond to transition point (i.e. EP) and at unbroken regime. The degree of squeezing is enriched significantly when the system is at unbroken phase. From the above expression, it is clear that degree of squeezing can also be manipulated by changing phase of the input state.

5.6.3 Principal and Normal squeezing

We examine the possibility of single mode squeezing via principal and normal squeezing. We derive the analytical expressions for principal and normal squeezing factors for both the passive and active cavity field mode by using equation (2.12) and (2.13) and solutions of equation (5.4).

$$P_s(a_1) = A_3^* A_3 |{\alpha_1}^2|^2 - |(A_1 A_3 {\alpha_1}^2 + 2A_3^2 {\alpha_1}^* {\alpha_1}^3 + A_1 A_6 \alpha_1 \alpha_2 + A_1 A_7 {\alpha_1}^2 + 2A_1 A_8 {\alpha_1}^* {\alpha_1}^3)| \quad (5.12)$$

$$N_s(a_1) = A_3^* A_3 |{\alpha_1}^2|^2 - Re(A_1 A_3 {\alpha_1}^2 + 2A_3^2 {\alpha_1}^* {\alpha_1}^3 + A_1 A_6 \alpha_1 \alpha_2 + A_1 A_7 {\alpha_1}^2 + 2A_1 A_8 {\alpha_1}^* {\alpha_1}^3) \quad (5.13)$$

$$P_s(a_2) = 0 \text{ and } N_s(a_2) = 0 \quad (5.14)$$

Equation (5.12) and (5.13) are plotted in figure 5.5 (a) and (b), respectively. The negativity of $P_s(a_1)$ indicates the possibility of principal squeezing of the field mode a_1. The degree of nonclassicality is slightly higher for PACS. Again, the temporal variation of normal squeezing factor shows that $N_s(a_1)$ positive up-to $Ut \approx 0.75$. If the value of Ut increases further the value of $N_s(a_1)$ is negative. This gives the

signature of normal squeezing. The negative value of normal squeezing factor is small for $k_2/k_1 = -0.2$ and increases when gain-to-loss ratio becomes $k_2/k_1 = -0.5$. From equation (5.14) it is clear that both principal and normal squeezing is not possible for active cavity field mode. This is also well established via quadrature squeezing (in sub-section 5.6.1).

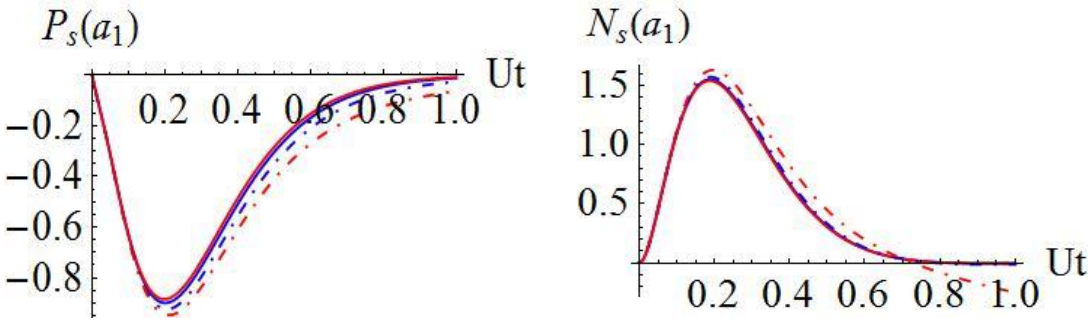

(a) (b)

Figure 5.5: Plot of (a) $P_s(a_1)$ with normalised time Ut for $k_2/k_1 = 0.5$ (red line), $k_2/k_1 = 0.2$ (blue line), $k_2/k_1 = -0.2$ (blue dot-dashed line) and $k_2/k_1 = -0.5$ (red dot-dashed line) (b) $N_s(a_1)$ with normalised time Ut for $k_2/k_1 = 0.2$ (blue line), $k_2/k_1 = 0.5$ (red line), $k_2/k_1 = -0.2$ (blue dot-dashed line) and $k_2/k_1 = -0.5$ (red dot-dashed line). The other parameters are $|\alpha_1| = 2, |\alpha_2| = 1,\ J/k_1 = 0.5$.

The analytic expressions of passive-active compound mode squeezing factors $P_s(a_1a_2)$ and $N_s(a_1a_2)$ are obtained by using equation (2.14) and (2.15) and solutions of equation (5.4) as follows

$$P_s(a_1a_2) = A_3^*A_3|{\alpha_1}^2|^2 - |(A_1A_3{\alpha_1}^2 + 2A_3^2{\alpha_1}^*{\alpha_1}^3 + A_1A_6\alpha_1\alpha_2 + A_1A_7{\alpha_1}^2 + 2A_1A_8{\alpha_1}^*{\alpha_1}^3 + A_2B_3{\alpha_1}^2 + A_1B_4{\alpha_1}^2)| \quad (5.15)$$

$$N_s(a_1a_2) = A_3^*A_3|{\alpha_1}^2|^2 - Re(A_1A_3{\alpha_1}^2 + 2A_3^2{\alpha_1}^*{\alpha_1}^3 + A_1A_6\alpha_1\alpha_2 + A_1A_7{\alpha_1}^2 + 2A_1A_8{\alpha_1}^*{\alpha_1}^3 + A_2B_3{\alpha_1}^2 + A_1B_4{\alpha_1}^2) \quad (5.16)$$

The time evolution of squeezing factors $P_s(a_1a_2)$ and $N_s(a_1a_2)$ are depicted in figure 5.6 (a, b). The negative regions of $P_s(a_1a_2)$ indicate the signature of compound mode

principal squeezing. The degree of squeezing is more for PACS and it is also increases with gain-to-loss ratio. From figure 5.6(b), it is clear that compound mode normal squeezing is not possible for passive-passive cavity configuration. The normal squeezing factor $N_s(a_1a_2)$ is negative for normalised time $Ut \geq 0.7$. These variations are similar to single field mode but the degree of both the squeezing is enhanced for compound field mode.

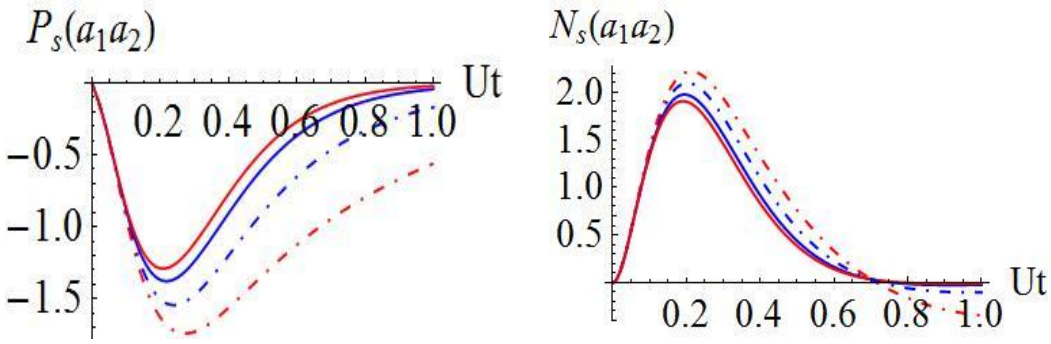

(a) (b)

Figure 5.6: Plot of (a) $P_s(a_1a_2)$ with normalised time Ut for $k_2/k_1 = 0.5$ (red line), $k_2/k_1 = 0.2$ (blue line), $k_2/k_1 = -0.2$ (blue dot-dashed line) and $k_2/k_1 = -0.5$ (red dot-dashed line) (b) $N_s(a_1a_2)$ with normalised time Ut for $k_2/k_1 = 0.2$ (blue line), $k_2/k_1 = 0.5$ (red line), $k_2/k_1 = -0.2$ (blue dot-dashed line) and $k_2/k_1 = -0.5$ (red dot-dashed line). The other parameters are $|\alpha_1| = 2, |\alpha_2| = 1, J/k_a = 0.5$.

To study the effect of driving term, we have numerically worked out the system Hamiltonian by using master equation approach and studied the quadrature variation with different system parameters. Figure 5.7 (a) and (b) display the varation of the variance of the field quadratures with normalised cavity detuning for gain-to-loss ratio $k_2/k_1 = 0.2$ and $k_2/k_1 = -0.2$. It is observed that degree of squeezing is enhanced for PACS which is also same for analytical results. The degree of squeezing also depends on photon tunnelling strength between the cavities. The quadrature variation with nonlinear strength is depicted in figure 5.7 (c), at zero cavity detuning. The

squeezing effect attains maximum value when normalised nonlinear strength is nearly equal to 0.1, which is well satisfied by experimental system of micro-toroid setup with silica glass material [186].

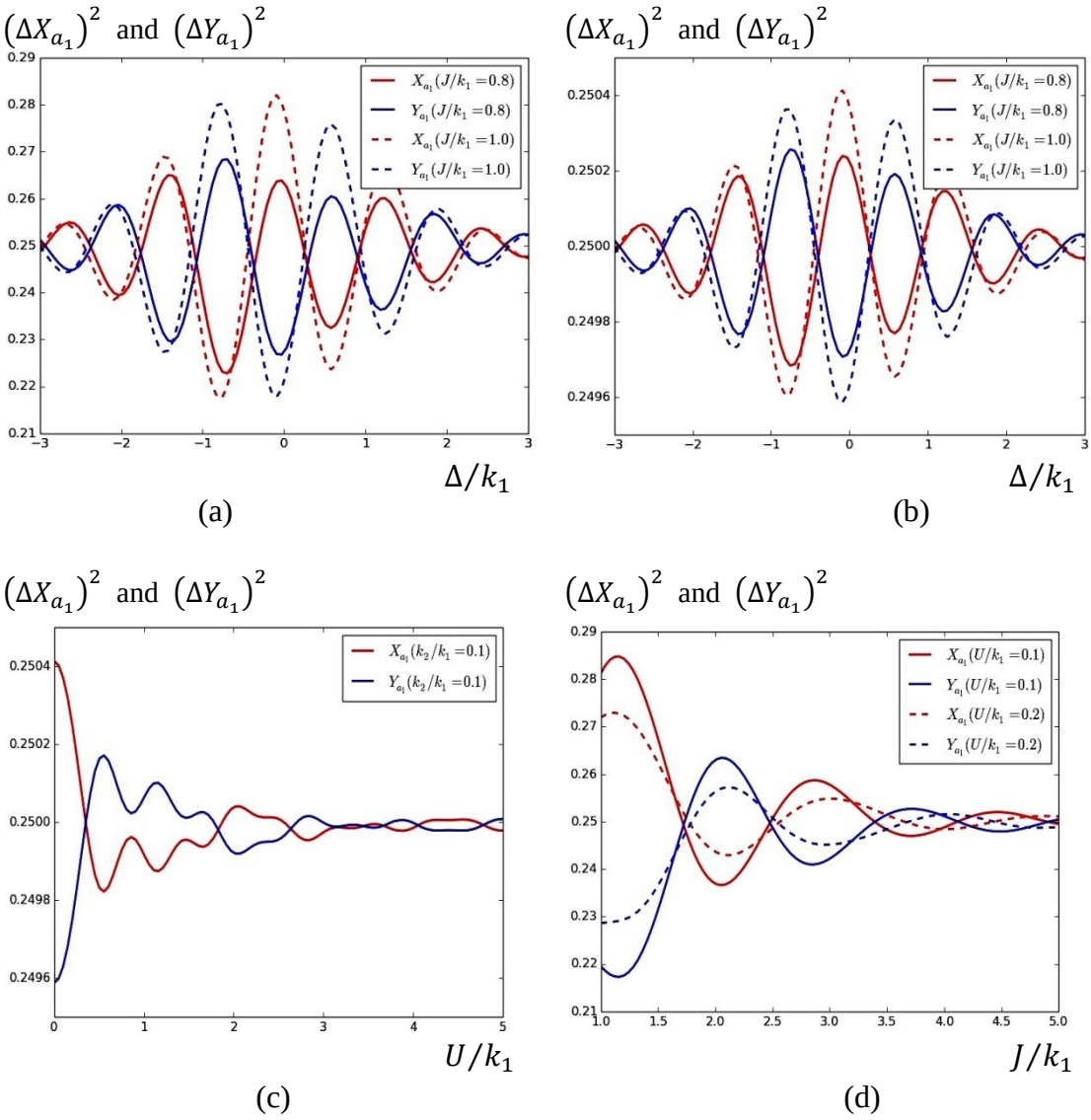

Figure 5.7: Variation of $(\Delta X_{a_1})^2$ and $(\Delta Y_{a_1})^2$ with (a-b) cavity detuning Δ/k_1 for different values of normalised photon tunnelling strength J/k_1. The gain-to-loss ratio $k_2/k_1 = 0.2$ and $k_2/k_1 = -0.2$ (c) nonlinear strength U/k_1 for different values of gain-to-loss ratio k_2/k_1 , $\Delta/k_1 = 0$ and $J/k_1 = 1$ (d) normalized photon tunnelling strength J/k_1 for different values of U/k_1, $\Delta/k_1 = 0$ and $k_2/k_1 = 0.1$. The normalised driving strength is $\Omega/k_1 = 0.01$.

Figure 5.7 (d) represents the variation as a function of normalised photon tunnelling strength at resonance. The optimum squeezing is possible for $J/k_1 \sim 1$ and beyond that region degree of squeezing is decreases monotonically.

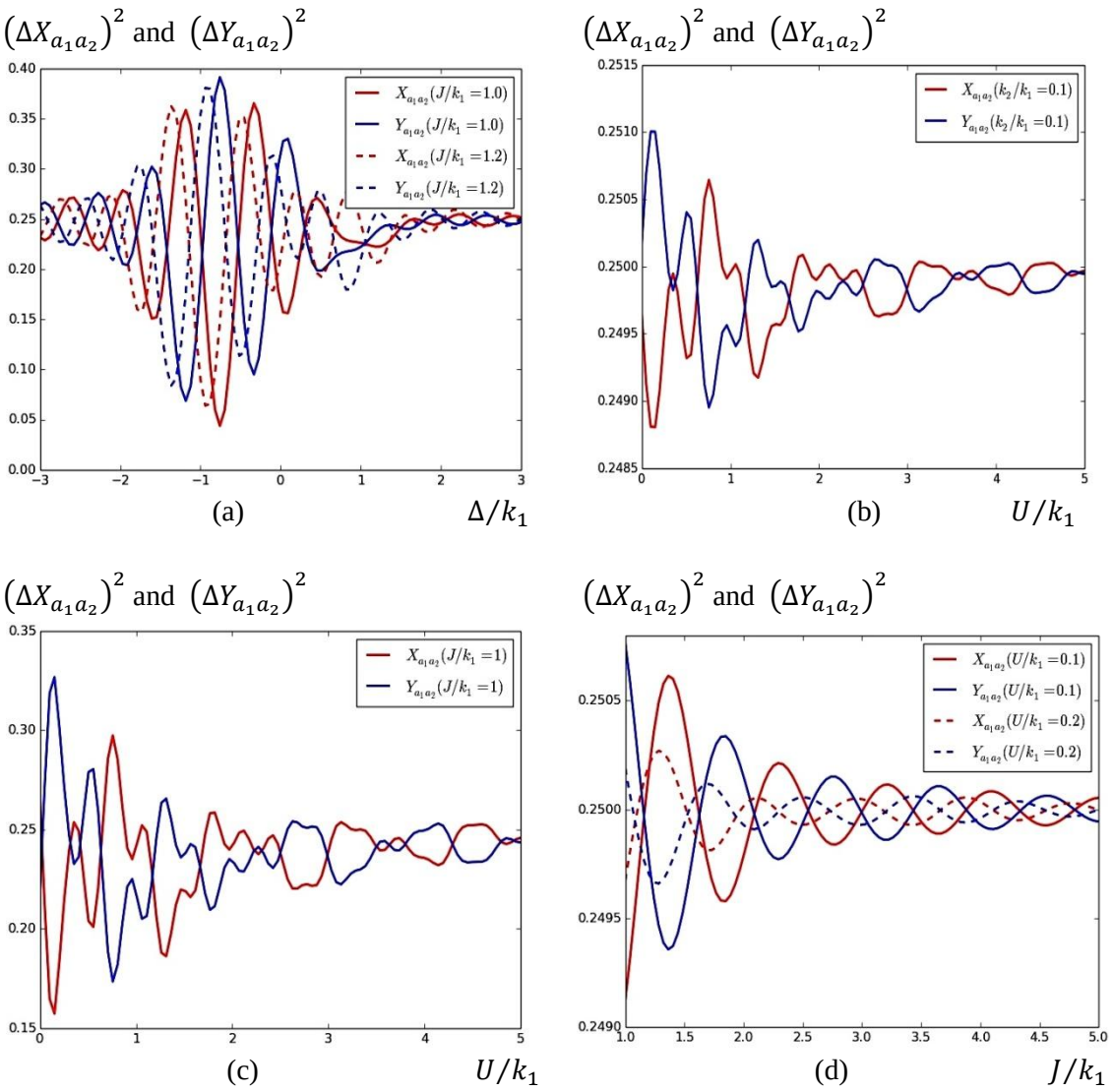

Figure 5.8: Variation of $(\Delta X_{a_1a_2})^2$ and $(\Delta Y_{a_1a_2})^2$ with (a) cavity detuning Δ/k_1 for different values of photon tunnelling strength J/k_1 and $k_2/k_1 = -0.2$ (b) nonlinear strength U/k_1 for $\Delta/k_1 = 0$ and $k_2/k_1 = 0.2$ (c) nonlinear strength U/k_1 for $\Delta/k_1 = 0$ and $k_2/k_1 = -0.2$ (d) normalised photon tunnelling strength J/k_1 for different values of U/k_1, $\Delta/k_1 = 0$ and $k_2/k_1 = 0.1$. The normalised driving strength is $\Omega/k_1 = 0.01$.

The quadrature variations of compound field mode as a functions of system parameters are shown in figure 5.8 (a-d), in presence of cavity driving term. Figure 5.8(a) displays the variation with cavity detuning for PACS. The fluctuation of the field quadratures attains maximum around $\Delta/k_1 = 0$ i.e. at resonance condition. The fluctuation of the field quadrature gradually decays when cavity detuning is far away from resonance. Figure 5.8(b) and (c) shows the fluctuation as a function of normalised Kerr nonlinear strength for PPCS and PACS. The degree of squeezing is significantly enhanced for PACS. The quadrature variation with photon tunnelling strength is depicted in figure 5.8(d). The variation is same as single mode squeezing.

5.7 Intermodal entanglement

Here, we have analyzed lower as well as higher order entanglement between two cavity field modes. How the degree of entanglement influenced at EP, is also reported.

5.7.1 Lower order entanglement

To illustrate the possibility of lower order squeezing by two inseparability criteria, Duan et al criteria and Hillery-Zubairy criteria. First we have found out entanglement parameter by analytical solutions of equation (5.4) and then numerically by master equation approach. According to Duan et al criteria (equation 2.26), we obtain the following expression of entanglement correlation parameter as follows:

$$e_{a_1a_2} = A_2^*A_2 + 2A_3^*A_3|\alpha_1|^2(1+2|\alpha_1|^2) + B_2^*B_2 + (A_1^*A_4 + B_1^*B_3 + A_2^*B_1 + 2A_1^*A_3|\alpha_1|^2 + 2A_1^*A_5\alpha_1\alpha_2{}^* + A_1^*A_6\alpha_1{}^*\alpha_2 + 2A_1^*A_7|\alpha_1|^2 + 3A_1^*A_8|\alpha_1{}^2|^2 + 2A_1^*B_4|\alpha_1|^2 + 2A_3^*B_2|\alpha_1|^2 + A_6^*B_1|\alpha_1|^2 + c.c.) \quad (5.17)$$

The right side of the expression (5.17) is plotted with normalised time Ut , in figure 5.9 (a-f). Figure 5.9(a) and (b) represent the entanglement factor for PPCS and PACS at

broken phase, respectively. As the value of $e_{a_1a_2}$ is positive, so entangled state is not possible for PPCS. Again, the negativity of $e_{a_1a_2}$ indicates the possibility of nonseperable state for PACS.

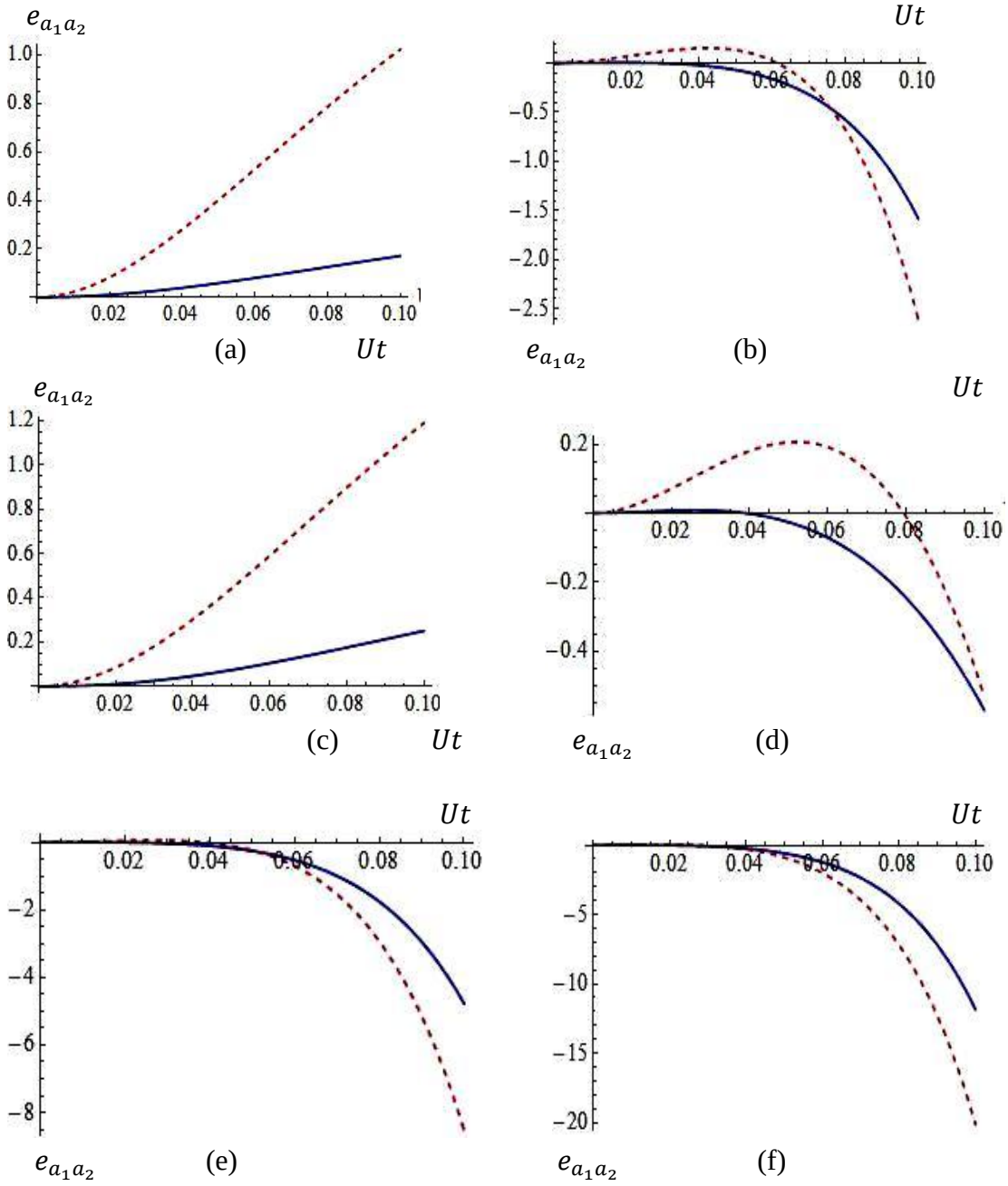

Figure 5.9: Variation of $e_{a_1a_2}$ with normalised time Ut for $U/k_1 = 0.1$, $|\alpha_1| = 2$, $|\alpha_2| = 1$ (blue solid line);$|\alpha_1| = 3$, $|\alpha_2| = 1$(red dashed line) with (a) $J/k_1 = 0.2$, $k_2/k_1 = 3$ (b) $J/k_1 = 0.2$, $k_2/k_1 = -3$ (c) $J/k_1 = 0.5$, $k_2/k_1 = 3$ (d) $J/k_1 = 0.5$, $k_2/k_1 = -1$ (e) $J/k_1 = 0.5$, $k_2/k_1 = -3$ (f) $J/k_1 = 1.0$, $k_2/k_1 = -3$.

Figure 5.9(c), (d) and (e), present the same variations at EP. For passive-passive configuration there is no signature of entanglement as the right side of equation (5.17), always positive, as shown in figure 5.9(c). On the other hand, the negative regions (figure 5.9d and e) of the entanglement factor give the signature of entanglement for passive-active system. The degree of squeezing increases with gain-to-loss ratio. Figure 5.9(f) displays the variation for PACS at unbroken $\mathcal{PT}$ −symmetry phase. The negativity of $e_{a_1a_2}$ is enhanced significantly at unbroken regime as compared to other two. The degree of non-separability also depends on weight factor of the input field.

We have examined the possibility of non-separable state by another moment based criteria, Hillery-Zubairy criteria (equation 2.28). Using above criteria and solutions of equation (5.4), we have derived the following expression of $E_{a_1a_2}$.

$$E_{a_1a_2} = A_3^* A_3 |\alpha_1{}^2|^2 |\alpha_2|^2 + (B_1^* B_4 \alpha_1{}^* \alpha_2 \alpha_1{}^2 + c.c.) \qquad (5.18)$$

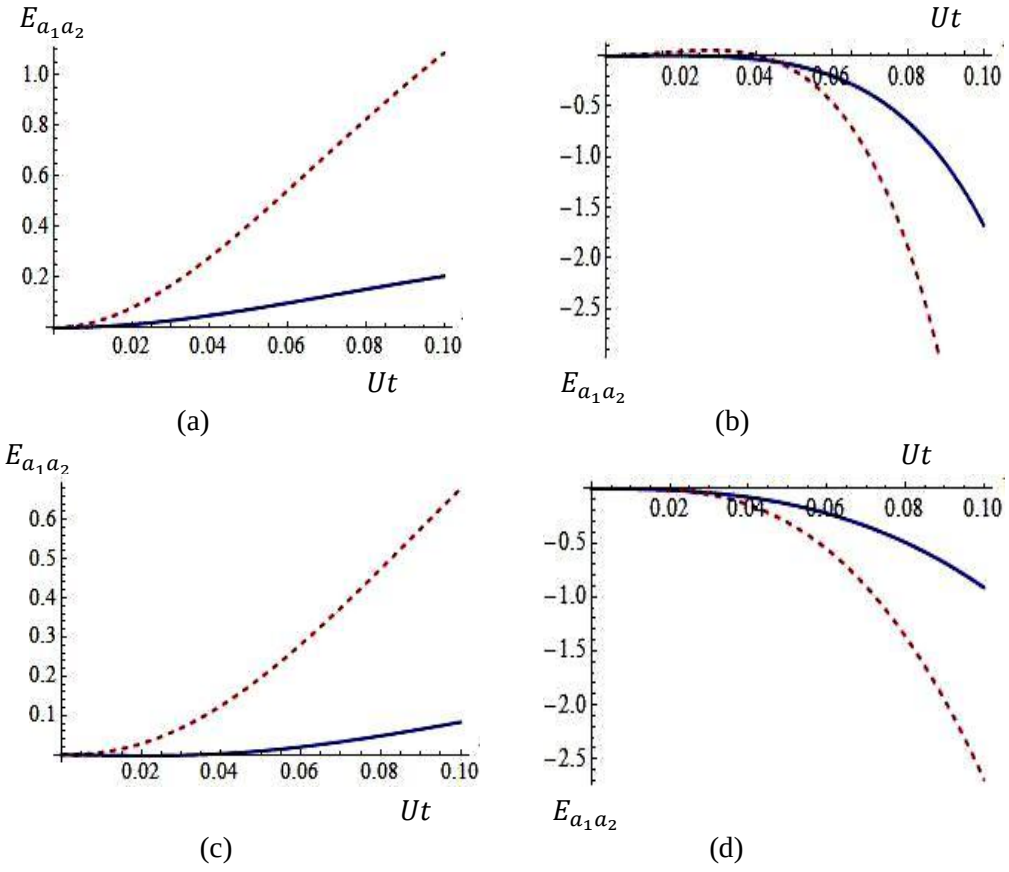

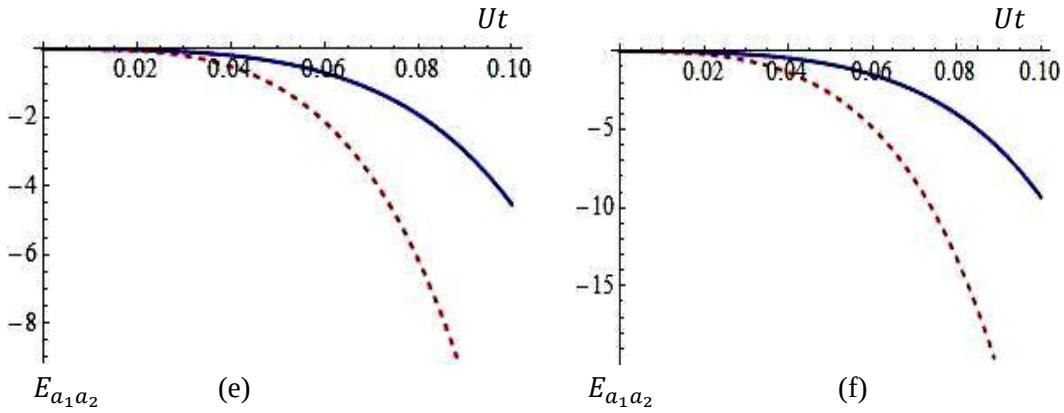

Figure 5.10: Variation of $E_{a_1a_2}$ with normalised time Ut for $|\alpha_1| = 2$, $|\alpha_2| = 1$ (blue solid line); $|\alpha_1| = 3$, $|\alpha_2| = 1$ (red dashed line) (a) $J/k_1 = 0.2$, $k_2/k_1 = 3$ (b) $J/k_1 = 0.2$, $k_2/k_1 = -3$ (c) $J/k_1 = 0.5$, $k_2/k_1 = 3$ (d) $J/k_1 = 0.5$, $k_2/k_1 = -1$ (e) $J/k_1 = 0.5$, $k_2/k_1 = -3$ (f) $J/k_1 = 1.0$, $k_2/k_1 = -3$.

The expression of $E_{a_1a_2}$ is not simple, so we plot it as a function of time, in figure 5.10 (a-f). The plots of $E_{a_1a_2}$ is similar to the plots (Figure 5.9) as obtained from Duan et al criteria and the variations are similar. But degree of non-separability is little different.

We find out entanglement correlation parameters numerically, in presence of driving term by using Duan et al criteria and plot these in figure 5.11. Figure 5.11 (a) and (b) display the variation of $e_{a_1a_2}$ as a function of cavity detuning at EP, for PPCS and PACS, respectively. For PPCS the negative value of $e_{a_1a_2}$ is very small i.e. weaker nonclassicality. For PACS negativity of $e_{a_1a_2}$ is increased and hence degree of entanglement is enhanced. This enhancement is also significant when k_2/k_1 changed from -1 to -2 . So, one can control the degree of non-separability by changing gain-to-loss ratio. Figure 5.11(c) and (d) represent the variation with different values of photon tunnelling strength and Kerr nonlinear strength. For strength of nonlinearity $U/k_1 = 0.1$ the degree of non-separability is optimum. The degree of non-separability decreases when the strength of nonlinearity in the PPCS increases.

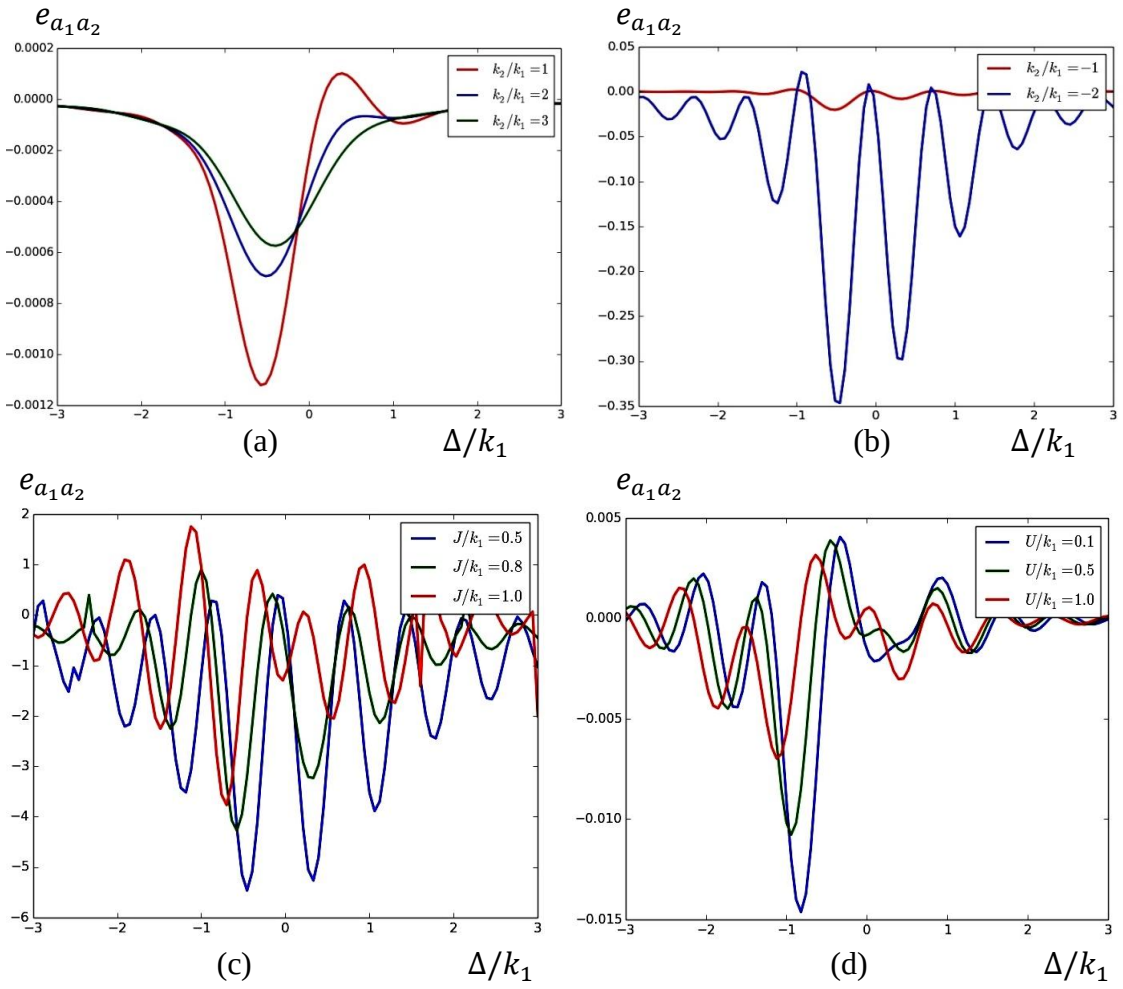

Figure 5.11: Plot of $e_{a_1a_2}$ with cavity detuning Δ/k_1 for $\Omega/k_1 = 0.01$ (a)-(b) $U/k_1 = 0.1$ and $J/k_1 = 0.5$ (c) $k_2/k_1 = -1$ and $U/k_1 = 0.1$ and (d) $k_2/k_1 = -1$ and $J/k_1 = 0.5$.

5.7.2 Higher order entanglement

We have analyzed the possibility of higher order entanglement using Hillery-Zubairy criteria and Agarwal-Biswas criteria, via analytically and numerically, respectively. First, we have derived the analytical expression of entanglement factor $E_{a_1a_2}(m,n)$, using Hillery-Zubairy criteria (equation 2.31).

$$E_{a_1a_2}(m,n) = m^2 A_3^* A_3 |{\alpha_1}^2|^{m+1} |\alpha_2|^{2n}$$
$$-(mnB_1^* B_4 {\alpha_1}^{*m} {\alpha_1}^{m+1} {\alpha_2}^{*n} {\alpha_2}^{n-1} + c.c.) \qquad (5.19)$$

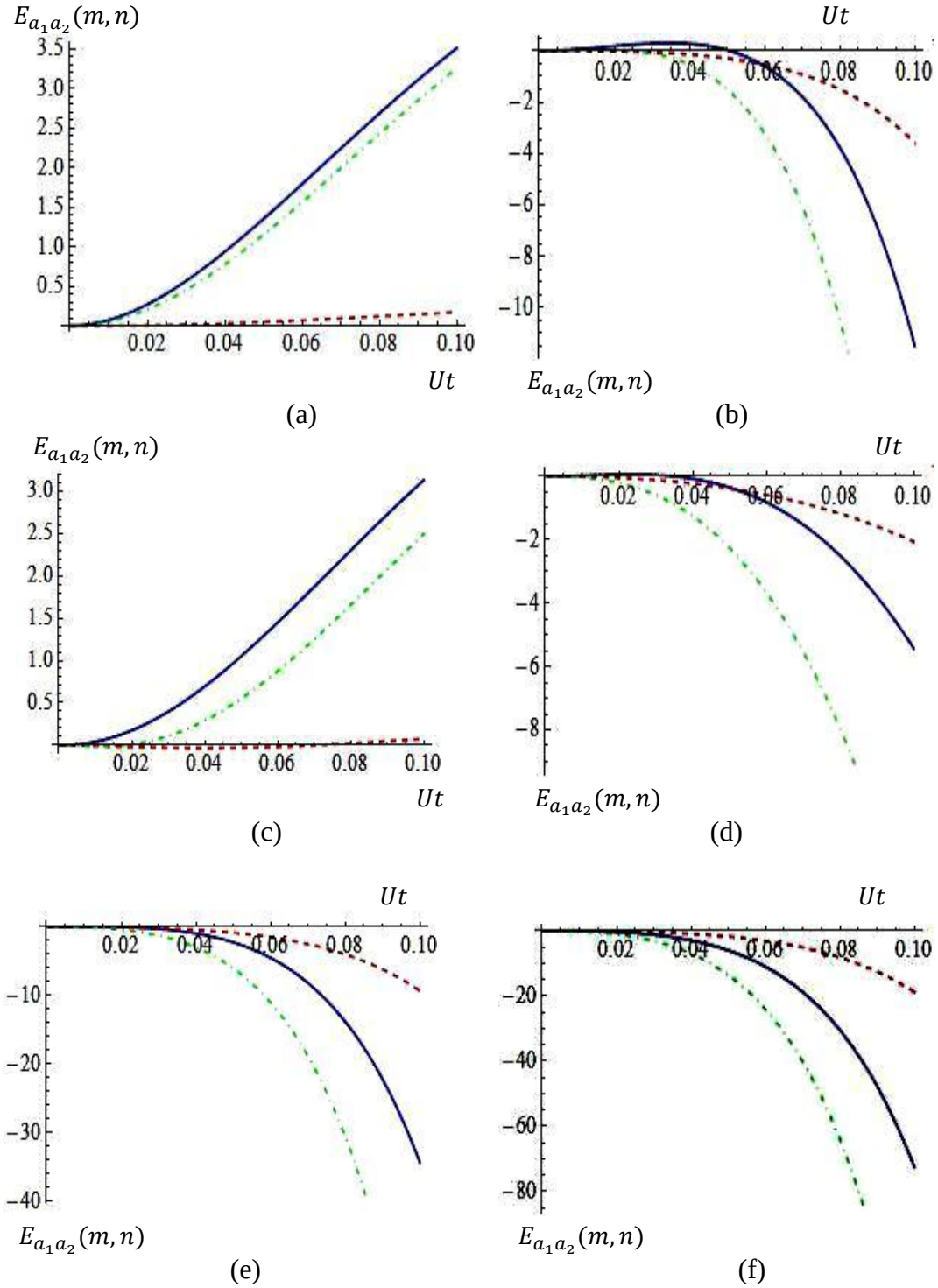

Figure 5.12:Variation of $E_{a_1a_2}(m,n)$ with normalised time Ut for $U/k_1 = 0.1$, $\alpha_1 = 2$, $\alpha_2 = 1$, $m = 2$, $n = 1$ (blue solid line), $m = 2$, $n = 2$ (green dot-dashed line) and $m = 1$, $n = 2$ (red dashed line) (a) $J/k_1 = 0.2$, $k_2/k_1 = 3$ (b) $J/k_1 = 0.2$, $k_2/k_1 = -3$ (c) $J/k_1 = 0.5$, $k_2/k_1 = 3$ (d) $J/k_1 = 0.5$, $k_2/k_1 = -1$ (e) $J/k_1 = 0.5$, $k_2/k_1 = -3$ (f) $J/k_1 = 1.0$, $k_2/k_1 = -3$.

Temporal variation of equation (5.19) is displayed in figure 5.12 (a-f). The value of $E_{a_1a_2}(m,n)$ is positive for PPCS for broken phase and at EP (figure 5.12a and c). These are similar for others as discussed in lower order entanglement (section 5.7). Here, degree of entanglement is enhanced with order number. To explain, we assume $m = n$ (for simplicity) and put in above equation (5.19) and one can find that a term $m^2|{\alpha_1}^2|^m|\alpha_2|^m$ plays the role of amplification factor and hence enhances the degree.

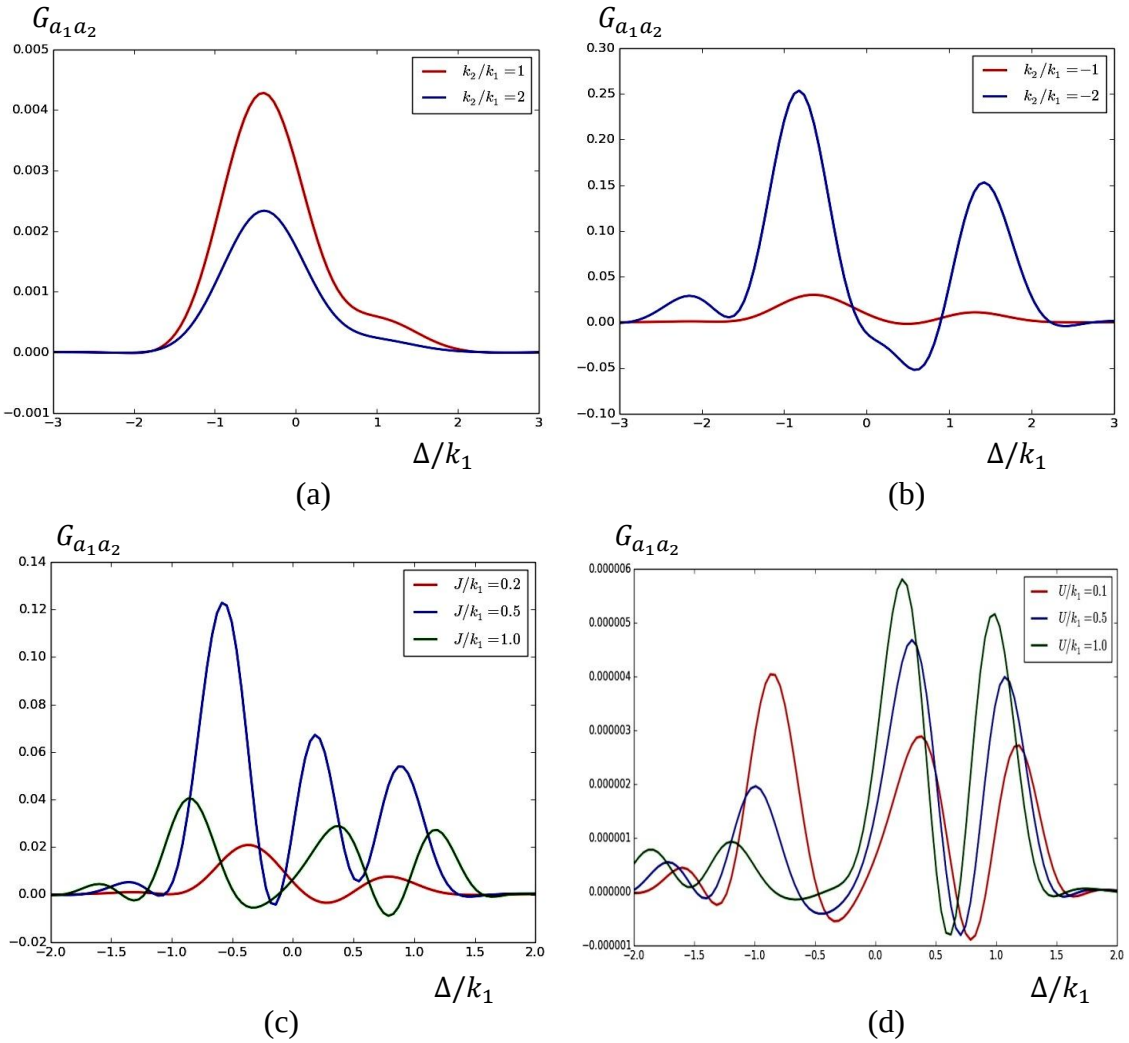

Figure 5.13: Plot of $G_{a_1a_2}$ with cavity detuning Δ/k_1 for $\Omega/k_1 = 0.01$ (a)-(b) $U/k_1 = 0.1$ and $J/k_1 = 0.5$ (c) $k_2/k_1 = -1$ and $U/k_1 = 0.5$ and (d) $k_2/k_1 = -1$ and $J/k_1 = 0.5$.

Using Agarwal-Biswas criteria (equation 2.32) – higher order correlation criteria of two mode non-separable states and master equation (5.6), we plot $G_{a_1a_2}$ as a function of

cavity detuning with different system parameters as shown in figure 5.13 (a-d). Figure 5.13(a) indicates that $G_{a_1a_2}$ is positive, i.e. states are separable for PPCS. This result is similar with analytical solutions as obtained by using Duan et al criteria and Hillery-Zubairy criteria. For PACS the value of $G_{a_1a_2}$ is negative and negativity increases with negative values of gain-to-loss ratio. Variation of $G_{a_1a_2}$ for different J and U are shown in figure 5.13(c) and (d), respectively. The degree of separability is higher for $J/k_1 = 1$.

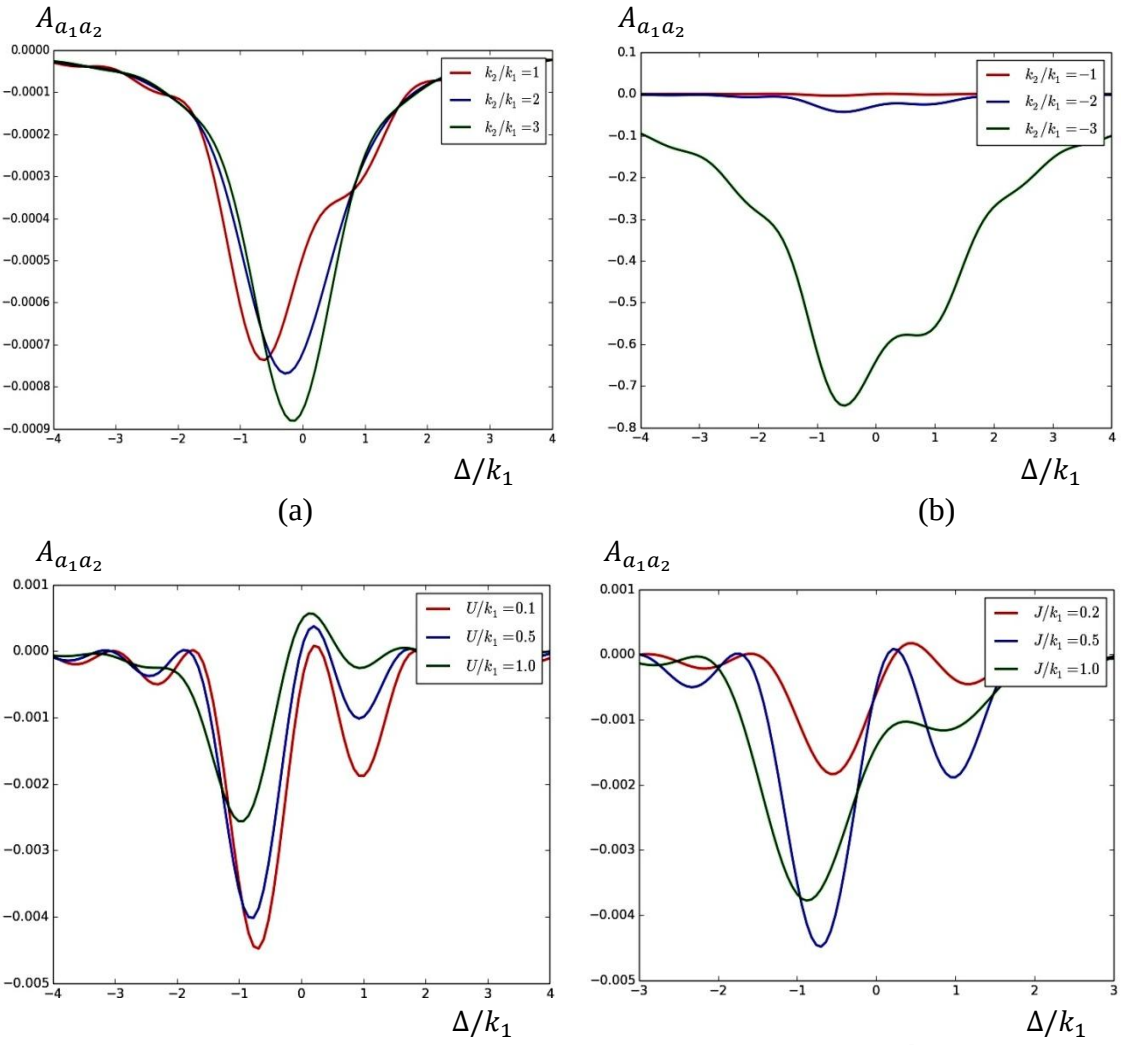

Figure 5.14: Plot of $A_{a_1a_2}$ with cavity detuning Δ/k_1 for $\Omega/k_1 = 0.01$ (a)-(b) $U/k_1 = 0.1$ and $J/k_1 = 0.5$ (c) $k_2/k_1 = -1$ and $J/k_1 = 0.5$ and (d) $k_2/k_1 = -1$ and $U/k_1 = 0.1$.

The possibility of entangled state in present system is also investigated by another higher order correlation function $A_{a_1 a_2}$ (Agarwal-Biswas criteria – equation 2.33). The variation of $A_{a_1 a_2}$ with normalised detuning is shown in figure 5.14 (a-d). Figure 5.14(a-b) present the variation for $k_2/k_1 = +ve$ and $k_2/k_1 = -ve$, respectively. Both the variation is shown that non-separable state is possible for PPCS and PACS. There is weaker nonclassicality for PPCS and comparatively stronger nonclassicality for PACS. Figure 5.14(c) displays the variation at EP for different nonlinearity and it is clear that the degree of nonclassicality is optimum for $U/k_1 = 0.1$. This is well established in analytical solution in previous section and also feasible with experimental setup. Figure 5.14(d) depicts the variation for different strength of photon tunnelling.

5.9 EPR steering

In this section, we have discussed about the possibility of steerable states. This is stronger correlation than entangled state. We have found out the steering correlation factor ξ_{ij} using master equation (5.6) and Cavalcanti et al criteria (equation 2.37). The numerical solution is obtained by Monte Carlo simulation.

In figure 5.15 (a) and (b), we display how the correlation factor ξ_{ij} explicitly depends on the cavity detuning Δ/k_1 for different gain-to-loss ratio k_2/k_1 for PACS and PPCS. Interestingly, for $a_1 a_2$ inter-mode ξ_{ij} is negative whereas for $a_2 a_1$ inter-mode ξ_{ij} is positive for PACS. On the other hand, ξ_{ij} is positive for either $a_1 a_2$ inter-mode or $a_2 a_1$ inter-mode in case of PPCS. This confirms the presence of asymmetric steering in the system. So, a_2 mode would be able to steer mode a_1 or vice-versa. This is important for quantum cryptography. The degree of steering is enriched for PACS as compared to PPCS.

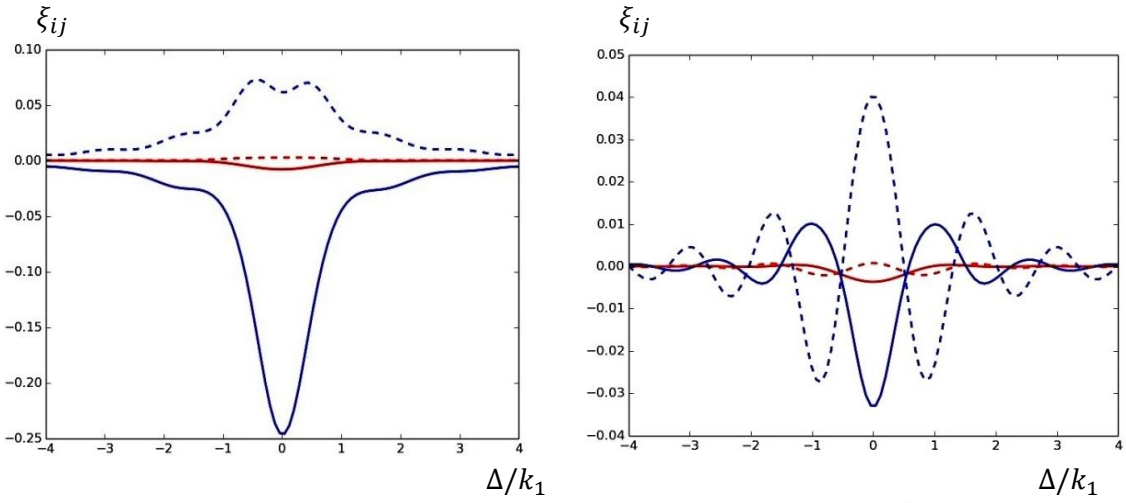

(a) (b)

Figure 5.15: Variation of ξ_{ij} with cavity detuning Δ/k_1 for $J/k_1 = 0.5$, $U/k_1 = 0.1$ and $\Omega/k_1 = 0.01$ (a) a_1a_2 mode with $k_2/k_1 = -1$ (red solid line), $k_2/k_1 = -3$ (blue solid line) and a_2a_1 mode with $k_2/k_1 = -1$ (red dashed line), $k_2/k_1 = -3$ (blue dashed line) (b) a_1a_2 mode with $k_2/k_1 = 1$ (red solid line), $k_2/k_1 = 3$ (blue solid line) and a_2a_1 mode with $k_2/k_1 = 1$ (red dashed line) and $k_2/k_1 = 3$(blue dashed line).

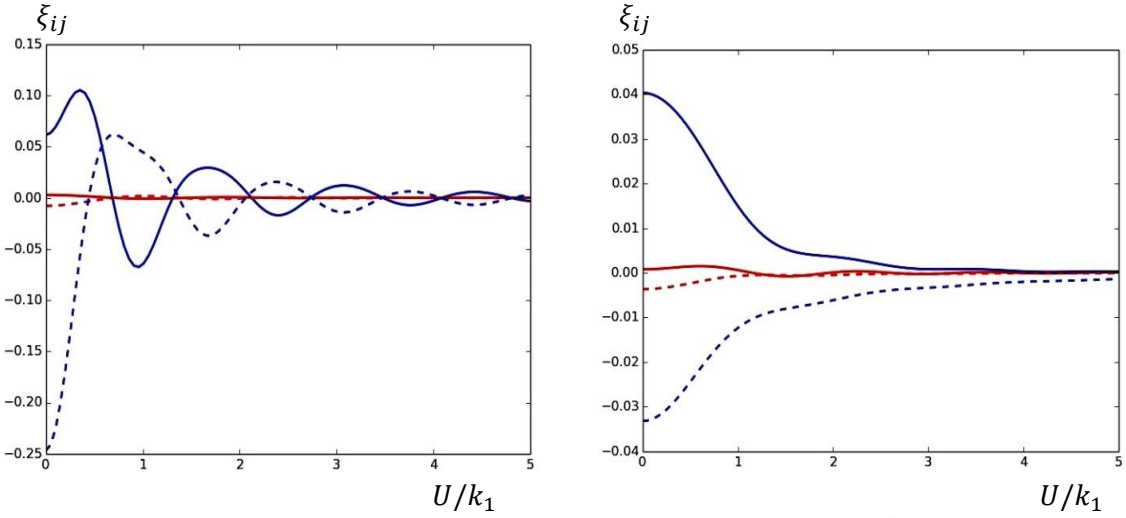

(a) (b)

Figure 5.16: Plot of ξ_{ij} with nonlinearity parameter U/k_1 for $J/k_1 = 0.5$, $\Delta = 0$ and $\Omega/k_1 = 0.01$ for (a) a_1a_2 mode with $k_2/k_1 = -1$ (red solid line) and $k_2/k_1 = -3$ (blue solid line) and a_2a_1 mode with $k_2/k_1 = -1$ (red dashed line) and $k_2/k_1 = -3$ (blue dashed line) (b) a_1a_2 mode with $k_2/k_1 = 1$ (red solid line) and $k_2/k_1 = 3$ (blue solid line) and a_2a_1 mode with $k_2/k_1 = 1$ (red dashed line) and $k_2/k_1 = 3$ (blue dashed line).

Figure 5.16 (a) and (b) depict the variation of ξ_{ij} as a function of nonlinear strength for different values of gain-to-loss ratio. Positive value of ξ_{ij} gives the signature of steerable state. The positivity is maximum around $U/k_1 \sim 0.1$, which is realizable in passive micro-toroid setup. Here the variation is of the asymmetric behaviour. The positive values of ξ_{ij} and hence the degree of steering is enhanced for $\mathcal{PT}$ −symmetry cavity system (PACS).

5.10 Summary

In this chapter, we have illustrated about $\mathcal{PT}$ −symmetry double cavity system. The system consists of two separated cavities, coupled via photon tunnelling. One is passive with optical Kerr medium and other is active cavity. The system Hamiltonian is solved analytically without driving by using Heisenberg EOM for both the field modes. To account the presence of driving term, we have also solved the system Hamiltonian numerically. Using both types of solution we have illustrated the possibilities of different nonclassicalities such as squeezing, entanglement and EPR steering.

From the analysis of various squeezing effects, it is revealed that squeezing is possible for passive cavity field mode but not for active mode. This result is also verified by using single mode principal and normal squeezing. The study of amplitude squared squeezing is shown where the degree of squeezing effects is enhanced as compared to lower order quadrature. Although, single active field mode squeezing is not possible but passive-active compound mode is possible. This is also confirmed by compound mode principal and normal squeezing.

The intermodal entanglement in the present system is studied via Duan et al criteria, Hillery-Zubairy criteria for lower order effects and Agarwal-Biswas criteria, Hillery-Zubairy criteria for higher order effects. The degree of intermodal noclassical effects

boost up higher order effects. The study of EPR steering indicates the presence of stronger correlation between the field modes as compared to entangled system. Interestingly, the present system gives the signature of asymmetric steering. This property has an important role in quantum computation.

The nonclassicalities are illustrated here to show prominent effect in unbroken $\mathcal{PT}$ −symmetry regime as compared to broken regime. The degree of both nonclassicalities studied here, are enhanced in PACS. It is also tuned by system parameters – weight factor and phase of the input state, photon tunnelling strength between the cavities, strength of nonlinearity in passive cavity and gain-to-loss ratio. The parameters used here, are experimentally realizable in micro-toroid setup. This study supplies a new platform to enhance the nonclassicalities via $\mathcal{PT}$ −symmetry architecture which is useful for nonclassical state generation.